
# DESIGN OPTIMIZATION STUDY ON AN ULTRAFAST SMART (SMA RESETTABLE) LATCH

**by**

**Shishira Nagesh**
**Won Hee Kim**

**ME 555-09-02**
**Winter 2009 Final Report**

## ABSTRACT

An active T-latch with automatic release and reset capabilities was designed and fabricated by Redmond et al. [1]. The latch demonstrated the technology for an automotive panel lockdown. The T-latch can be broadly divided into two parts based on the functionality of each. The first part consists of the shaft, shoulder, base and the ramps to be referred henceforth as the T-latch. The spool-packaged Shape Memory Alloy (SMA) actuator is the second component of the latch. The purpose of this optimization study is to make this device more suitable for use in the automotive sector where two of the main concerns are net volume (analogous to the weight) and power consumption of the device. An attempt will be made to optimize the T-latch for yet another important industry consideration, minimal footprint analogous to the packaging volume. Design tradeoffs and results are discussed for the individual subsystems and for the overall system.

# 1. Introduction

Latches are an essential machine element utilized by many sectors and there is a growing need for active latches with automatic release and reset capabilities. One such latch was designed by Redmond et al. [1]. The applications of the latch can be many, for example, as a hood-lift device for automobile panel. The T-latch is actuated with the help of SMA wires wound around a mandrel which is inherently connected to other parts of the T-latch. SMA wires are elegant solutions where a good force is required from a small volume of actuator package because of their high energy and power densities [1]. Due to its robust latching operation and use of a low power, high force actuator, the T-latch is a viable design to be integrated into automobile systems. A schematic diagram showing the various parts of the T, along with the intended division of the subsystems is given below.

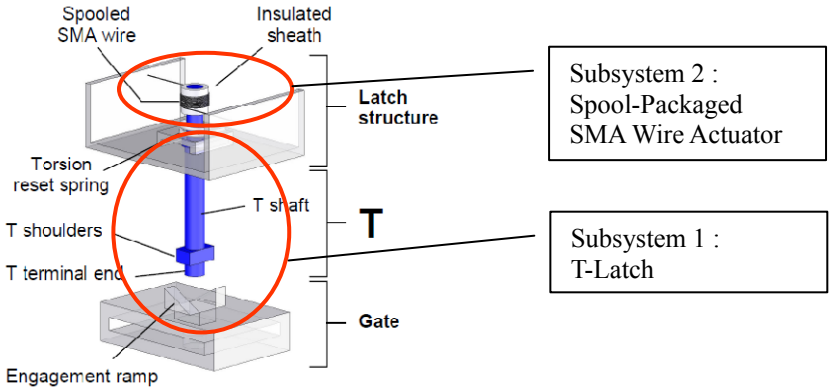


**Fig. 1.1 Diagram of SMART**

The first part of the project deals with optimizing the latch architecture (excluding the spool) for minimum net volume. The optimization is constrained by stress and geometric constraints that the dimensions of the T must be able to satisfy to ensure functionality. The second component of the project deals with optimizing the spool architecture for minimum power consumption. The SMA wires used to reset the latch require current to produce useful work and hence consume power. Redmond et al. [2] describe a novel approach toward packaging of SMA in the form of wire spools. The goal of the second optimization study is to minimize the power drawn by the wires while ensuring sufficient delivery of force required for resetting the latch. The optimization approach towards the combined system is to reduce the footprint of the device.

## 1.1.Nomenclature

Listed in the Table 2.1 are all the symbols and their respective units that will be used in this optimization study. The physical relevance of some of the symbols can sought from Fig. 2.1.

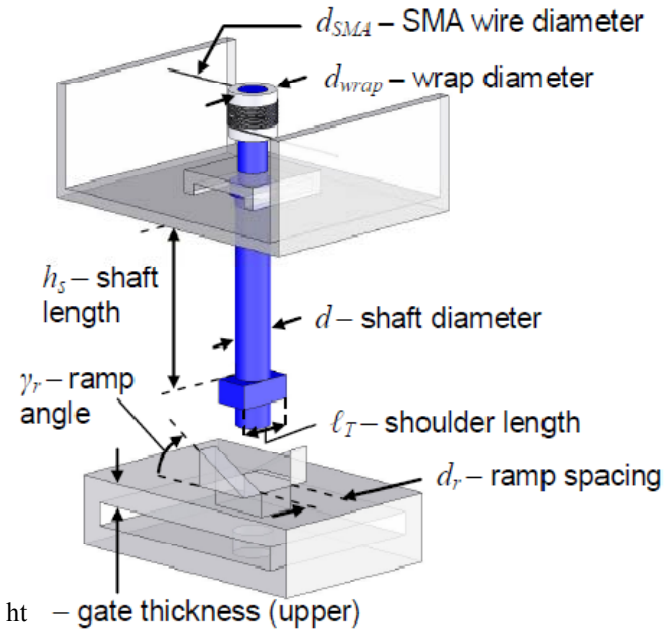


**Fig. 1.2 a Key Dimensions of the T-Latch**

**Table 2.1 List of symbols and units**

| No. | Symbol | Description | Unit |
|---|---|---|---|
| **1** | $d$ | shaft diameter | mm |
| **2** | $h_s$ | shaft length | mm |
| **3** | $l_t$ | shoulder length | mm |
| **4** | $b_t$ | shoulder breadth | mm |
| **5** | $h_t$ | shoulder height | mm |
| **6** | $d_r$ | ramp spacing | mm |
| **7** | $b_r$ | ramp breadth | mm |
| **8** | $\gamma$ | ramp angle | deg. |
| **9** | $t_r$ | ramp thickness | mm |
| **10** | $l_g$ | gate length | mm |
| **11** | $b_g$ | gate breadth | mm |

| | | | |
|---|---|---|---|
| **12** | $h_g$ | gate thickness | mm |
| **13** | $k_\Phi$ | reset spring stiffness | Nmm/deg |
| **14** | $\Phi_g$ | relative gate angle | deg. |
| **15** | $\Phi_{ko}$ | initial shoulder angle | deg. |
| **16** | $F_{sf}$ | seal force | N |
| **17** | $F_{sma}$ | SMA force | N |
| **18** | $F_{appe}$ | applied force (engagement) | N |
| **19** | $F_{appr}$ | applied force (retention) | N |
| **20** | $\mu_r$ | ramp-shoulder fric. coeff. | - |
| **21** | $\mu_g$ | gate-shoulder fric. coeff. | - |
| **22** | $s_t$ | seal thickness | mm |
| **23** | $d\_{wrap}$ | wrap dia. for SMA | mm |
| **24** | $\alpha$ | direction of $F_{appr}$ | deg. |
| **25** | $S_y$ | yield strength | MPa |
| **26** | $\sigma$ | normal stress | $N/m^2$ |
| **27** | $\tau$ | shear stress | $N/m^2$ |
| **28** | $\varepsilon$ | strain of SMA (martensite/austenite) | - |
| **29** | $V$ | packaging volume | $mm^3$ |
| **30** | $S_e$ | extended spring height | mm |
| **31** | $S_c$ | compressed spring height | mm |
| **32** | $S_d$ | exterior spring diameter | mm |
| **33** | $h_w$ | wrap height | mm |
| **34** | $f_{SMA}^{(M)}$ | material constitutive function (martensite) | |
| **35** | $f_{SMA}^{(A)}$ | material constitutive function (austenite) | |
| **36** | $\theta_w^{(M)}$ | wrap angle (martensite) | deg. |
| **37** | $\theta_w^{(A)}$ | wrap angle (austenite) | deg. |
| **38** | $\delta\phi$ | actuation angle | deg. |
| **39** | $\mu_{SMA}$ | friction coeff. between the SMA wire and the spool | |
| **40** | $d_{SMA}$ | diameter of SMA wire | mm/mil |
| **41** | $d_r$ | ramp spacing | mm |

| | | | |
|---|---|---|---|
| **42** | $\rho$ | curvature of the SMA wire ($d_{wrap}$ +1/2$d_{SMA}$) | mm |
| **43** | $\ell_{total}$ | total length of the SMA wire | mm |
| **44** | $\ell_w$ | wrap length of the SMA wire | mm |
| **45** | $\ell_{\mathrm{T}}$ | shoulder length of the T | mm |
| **46** | $\xi^{(M)}$ | martensite fraction of the SMA wire | |
| **47** | $\sigma_{tail}$ | stress of the SMA wire at the tail (non-wrap part) | MPa |

## 2. T-Latch (Subsystem 1) : *Shishira Nagesh*

### 2.1. Problem Statement

The SMA actuated latch was designed to be used primarily in automotive applications. Hence, minimizing the net volume with respect to the dimensions of the various components involved is one of the possible optimization studies which could further lead to reducing weight and in turn the fuel efficiency. In this sub-system, the net volume of the T-latch is minimized. Constraints for the optimization problem come from geometry and stress (yield and failure) criteria. While the stress constraints would want a sufficiently large diameter of the shaft of the latch to resist yield and failure, minimizing the net volume would entail as small a diameter as possible. A tradeoff is sought in the form of the optimization study.

### 2.2. Mathematical Model

#### 2.2.1. Objective Function

As mentioned in the problem statement, the objective function in this sub-system is *Packaging Volume* of the latch. This can be considered to be a sum of the individual volumes of the shaft, shoulder, ramps and gate. In terms of the symbols used above,

$$V = 1.05\frac{\pi d^2 h_s}{4} + l_t b_t h_t + b_r^2 t_r \tan(\gamma) + l_g b_g h_g - b_r d_r h_g$$

The first term in the objective function is the volume of the shaft which can be considered to be a cylinder. The length extending beyond the shoulders is assumed to be about 5% of the shaft height giving a factor of $1.05h_s$. The second, fourth and fifth terms are the volumes of the shoulder, gate and the hole in the gate (to make way for the shoulders to pass through) respectively, which can be considered to be cuboids. The third term is the combined volume of the two triangular ramps with a certain thickness.

#### 2.2.2. Constraints

The constraints used in modeling the T-latch are divided into Practical (Geometric) and Physical (Stress and Force balance) Constraints.

##### 2.2.2.1. Practical Constraints

Constraints that need to be satisfied in order for the design to be geometrically feasible

are listed below.

i) The shoulder length must be at least greater than or equal to the ramp spacing so that the shoulder does not just pass into the gap without making contact with the ramps.

$$l_t \geq d_r$$

ii) The gate must be at least as long as to support the two ramps and the spacing between them and the width of two springs attached to it and the spacing between them. The parameters of the spring like the exterior diameter, overall length and length when compressed were obtained from the McMaster-Carr catalogue for compression springs. A factor of 10% is assumed to be sufficient to space out the components.

$$l_g \geq 1.1\,(d_r + 2t_r + 2S_d)$$

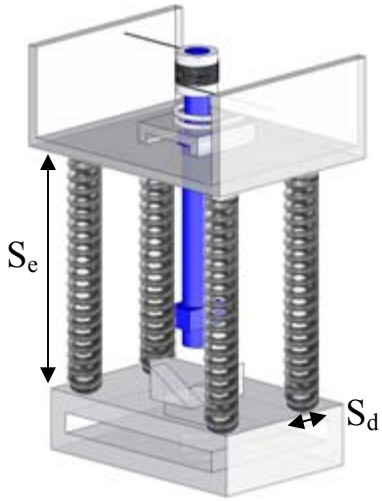


**Fig. 2.1 Spring Nomenclature**

iii) The shoulder width cannot hang over the ramps and must be within the breadth of the ramps.

$$b_t \leq b_r$$

iv) The breadth of the gate must be at least as wide as that of the ramp and the width of two springs to be able to support them. A factor of 10% is assumed to be sufficient to space out the components.

$$b_g \geq 1.1\,(b_r + 2S_d)$$

v) When the user presses down upon the latch, there must be no obstruction to the path of the shaft (though there must be some obstruction when there is no force being applied). So, the

breadth of the shoulder must be less than the ramp spacing. A factor of 10% is assumed for a good clearance.

$$1.1\, b_t \leq d_r$$

vi) The gate width must be at least equal to the shoulder length. This is because, when the shoulder rotates while being inserted into the gate, the shoulder length is along the width of the gate and the gate must be able to accommodate it.

$$b_g \geq l_t$$

vii) The breadth of the shoulder must be at least as big as the diameter of the shaft.

$$b_t \geq d$$

viii) During engagement, the shoulder length must be small enough to pass through the ramp breadth.

$$l_t \leq b_r$$

ix) The shaft diameter must be smaller than the ramp spacing in order to pass through it without any contact. A factor of 10% is assumed for a good clearance.

$$1.1\, d \leq d_r$$

x) The sum of the height of the shaft and the ramp height when the latch is not engaged, must be equal to the free length of the springs. This constraint written here for clarity but in the model execution, it is used to eliminate $\gamma_r$ to decrease the number of variables.

$$1.05\, h_s + b_r\, tan(\gamma_r) = S_e$$

xi) The shaft height after engaging the latch must be greater than the specified compressed length of the springs.

$$h_s \geq S_c$$

xii) The shaft height must be at least as large as to not fit fully inside the gate when the latch is engaged. So, it must be greater than the sum of the gate thickness and the ramp height.

$$h_s \geq h_g + b_r\, tan(\gamma_r)$$

### 2.2.2.2. Physical Constraints:

Some physical constraints, for the retention stage, based on yield strength and failure criteria, are described in [1]. These were arrived at by identifying points of maximum von Mises stress due to axial stress and transverse shear stress in the shaft (point A, Fig. 2.2a), maximum von Mises stress due to axial and bending stress in the shaft (point B), maximum transverse shear in the shoulder (datum C-C) and maximum bending stress in the shoulder (point D). These were identified for case where external force is applied in the plane of the shoulder and the shaft. A case of normal to shoulder was also analyzed. Points where maximum von Mises stress due to axial and transverse shear in the shaft act (point E, Fig. 2.2b) and maximum von Mises stress due to axial and bending stresses in the shoulder act (point F) were identified as critical. These are summarized in Table 2.1.

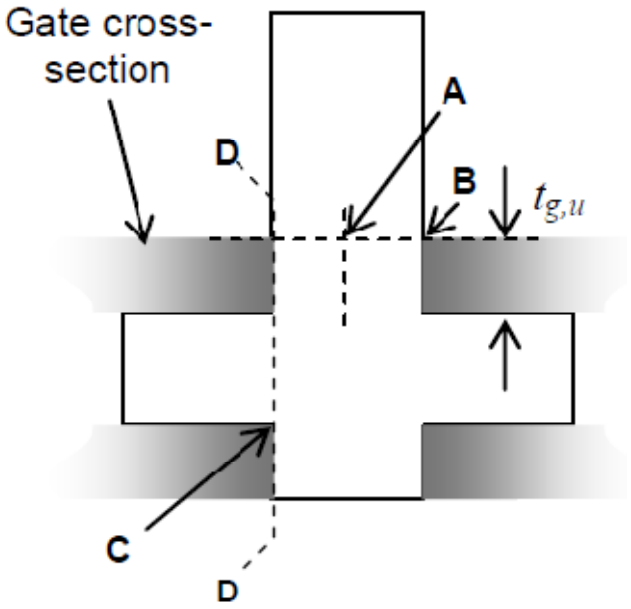


**Fig. 2.2a: Schematic of the T-latch with a general applied load for the plane of shoulder loading case and locations of the key stresses**

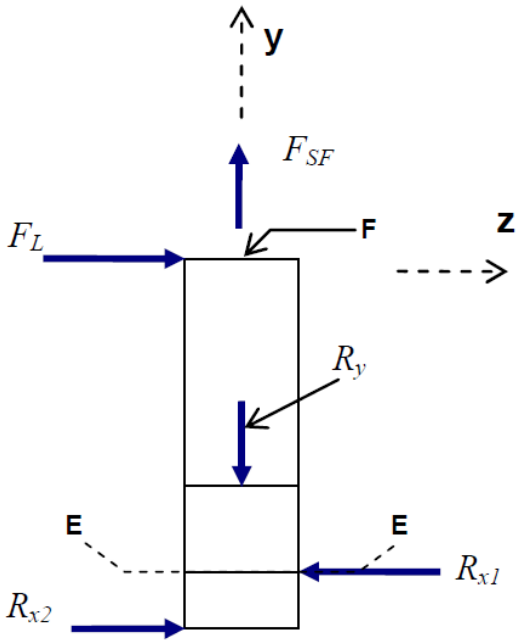


**Fig. 2.2b: Free body diagram for normal to shoulder loading of the T.**

**Table 2.1 Stress Constraints**

| | | Stress Constraint | Eq. |
|---|---|---|---|
| **Normal to shoulder loading model** | **Combine axial/transverse shear in shaft** | $S_y > \sigma_E = \sqrt{\left(\frac{F_{SF}}{\frac{1}{4}\pi d^2}\right)^2 + 3\left(\frac{16}{3\pi}\frac{F_{app}}{d^2}\right)^2}$ | 1 |
| | **Combined axial/bending in shaft** | $S_y > \sigma_F = \frac{32}{\pi}\frac{F_{app}(h_s + t_T)}{d^3} + \frac{F_{SF}}{\frac{1}{4}\pi d^2}$ | 2 |
| **Plane of shoulder loading model** | **Combined axial/transverse shear in shaft** | $S_y > \sigma_A = \sqrt{\left(\frac{F_{app}\cos\alpha + F_{SF}}{\frac{1}{4}\pi d^2}\right)^2 + 3\left(\frac{16}{3\pi}\frac{F_{app}\sin\alpha}{d^2}\right)^2}$ | 3 |
| | **Combined axial/bending in shaft** | $S_y > \sigma_B = \frac{F_{app}\cos\alpha + F_{SF}}{\frac{1}{4}\pi d^2} + \frac{32}{\pi}\frac{F_{app}\sin\alpha(h_s - t_{g,u})}{d^3}$ | 4 |
| | **Transverse shear stress in the shoulder** | $\frac{S_y}{2} > \tau_C = \frac{3}{4}\frac{(F_{SF} + F_{app}\cos\alpha)}{dt_T}$ | 5 |
| | **Bending stress in the shoulder** | $S_y > \sigma_D = \frac{3}{4}\frac{(F_{app}\cos\alpha + F_{SF})\left(\frac{\ell_T}{d} - 1\right)}{t_T^2}$ | 6 |

Other constraints arise from the torque requirement in the engagement and release stages. The moment the user must apply must be greater than the moment offered by the reset spring if engagement has to occur. This can be summarized as-

$$F_{app} \geq \frac{k_\varphi(\emptyset_g - \emptyset_{k0})}{\frac{1}{2}d_r}\frac{1 + \mu_r \tan\gamma_r}{\tan\gamma_r - \mu_r}$$

For this to be valid, the denominator of the equation must be greater than zero. This is also the definition of the coefficient of friction.

$$\tan\gamma_r - \mu_r \geq 0$$

To reset the latch, the moment from the SMA wire must be greater than the combined moment of the frictional force between the gate/shoulder and the reset spring.

$$F_{SMA} \geq \frac{k_\phi(\phi_g - \phi_{k0}) + \mu_g F_{SF}\frac{(\ell_T + d_r)}{4}}{d_{wrap}}$$

### 2.2.3. Design Variables and Parameters

Tables 2.2 and 2.3 show the 10 design variables and 13 parameters used in formulating the optimization problem. Since there is one equality constraint, *the number of degrees of freedom is 9.* The gate height ($h_g$) is assumed to be a parameter and is fixed at 5mm. A lower bound of 3 mm was assigned to all the design variables.

**Table 2.2 List of Variables with one feasible solution**

| No. | Symbol | Symbol Opt. | Description | Feasible Value |
|---|---|---|---|---|
| **1** | $d$ | $x_1$ | Shaft Diameter | 11.6 mm |
| **2** | $h_s$ | $x_2$ | Shaft Length | 26 mm |
| **3** | $l_t$ | $x_3$ | Shoulder Length | 13.6 mm |
| **4** | $b_t$ | $x_4$ | Shoulder Breadth | 13 mm |
| **5** | $h_t$ | $x_5$ | Shoulder Height | 4 mm |
| **6** | $b_r$ | $x_6$ | Ramp Breadth | 13.6 mm |
| **7** | $\gamma_r$ | $x_7$ | Ramp Angle | 29.52 deg |
| **8** | $l_g$ | $x_8$ | Gate Length | 60 mm |
| **9** | $b_g$ | $x_9$ | Gate Breadth | 50 mm |
| **10** | $d_r$ | $x_{10}$ | Ramp spacing | 13.6 mm |

**Table 2.3 List of Parameters with typical values**

| No. | *Symbol* | Description | Typical Value |
|---|---|---|---|
| **1** | $k_\Phi$ | Reset Spring Stiffness | 2.1 Nmm/deg |
| **2** | $\Phi_g$ | Relative Gate Angle | 30 deg |
| **3** | $\Phi_{ko}$ | Initial Shoulder Angle | 0 deg |
| **4** | $F_{sf}$ | Spring (Seal) Force | 75 N |
| **5** | $F_{sma}$ | SMA Force | 22 N |
| **6** | $F_{appe}$ | Applied Force (Engagement) | 20 kgf |
| **7** | $F_{appr}$ | Applied Force (Retention) | 3.55 kN |
| **8** | $\mu_r$ | Ramp Fric. Coeff. | 0.5 |

| | | | |
|---|---|---|---|
| **9** | $\mu_g$ | Gate Fric. Coeff. | 0.4 |
| **10** | $d_{wrap}$ | Wrap dia for SMA | 12.7 mm |
| **11** | $a$ | Angle of $F_{app}$ | 45 deg |
| **12** | $S_y$ | Yield Strength | 700 MPa |
| **13** | $h_g$ | Gate Thickness | 5 mm |
| **14** | $t_r$ | Ramp Thickness | 3 mm |
| **15** | $S_e$ | Extended Spring Length | 35 mm |
| **16** | $S_c$ | Compressed Spring Length | 26 mm |
| **17** | $S_d$ | Spring Outer Diameter | 14.3 mm |

### 2.2.4. Summary Model

The objective function along with the set of constraints is shown below.

**Minimize** V = $1.05\ \frac{\pi d^2 h_s}{4} + l_t b_t h_t + b_r^2 t_r \tan(\gamma) + l_g b_g h_g - b_r d_r h_g$

$\underline{x} \geq 3mm$

**Subject to**:

1. $d_r - l_t \leq 0$
2. $1.1\ (d_r + 2t_r + 2S_d) - l_g \leq 0$
3. $b_t - b_r \leq 0$
4. $1.1\ (b_r + 2S_d) - b_g \leq 0$
5. $1.1\ b_t - d_r \leq 0$
6. $l_t - b_g \leq 0$
7. $d - b_t \leq 0$
8. $l_t - b_r \leq 0$
9. $1.1\ d - d_r \leq 0$
10. $1.05\ h_s + b_r\ tan(\gamma_r) - S_e = 0$
11. $S_c - h_s \leq 0$
12. $h_g + b_r\ tan(\gamma_r) - h_s \leq 0$
13. $\mu_r - tan(\gamma_r) \leq 0$

14. $$\sigma_E = \sqrt{\left\{\frac{F_{SF}}{\frac{1}{4}\pi \mathrm{d}^2}\right\}^2 + 3\left\{\frac{16F_{app}}{3\pi \mathrm{d}^2}\right\}^2} - S_y \leq 0$$

15. $$\sigma_F = \frac{32}{\pi}\frac{F_{appr}(h_s + h_t)}{d^3} + \frac{F_{SF}}{\frac{1}{4}\pi \mathrm{d}^2} - S_y \leq 0$$

16. $$\sigma_A = \sqrt{\left\{\frac{F_{appr}\cos a + F_{SF}}{\frac{1}{4}\pi \mathrm{d}^2}\right\}^2 + 3\left\{\frac{16}{3\pi}\frac{F_{appr}\sin a}{\mathrm{d}^2}\right\}^2} - S_y \leq 0$$

17. $$\sigma_B = \frac{F_{appr}\cos a + F_{SF}}{\frac{1}{4}\pi \mathrm{d}^2} + \frac{32}{\pi}\frac{F_{appr}\sin a\,(h_s - h_g)}{d^3} - S_y \leq 0$$

18. $$\zeta_C = \frac{3}{4}\frac{F_{appr}\cos a + F_{SF}}{d h_t} - \frac{S_y}{2} \leq 0$$

19. $$\sigma_D = \frac{3}{4}\frac{\left(F_{appr}\cos a + F_{SF}\right)\left(\frac{l_t}{d} - 1\right)}{{h_t}^2} - S_y \leq 0$$

20. $$\frac{k_\varphi\left(\emptyset_g - \emptyset_{k0}\right)}{\frac{1}{2}d_r}\frac{1 + \mu_r \tan\gamma_r}{\tan\gamma_r - \mu_r} - F_{appe} \leq 0$$

21. $$\frac{k_\phi\left(\phi_g - \phi_{k0}\right) + \mu_g F_{SF}\frac{(\ell_T + d_r)}{4}}{d_{wrap}} - F_{SMA} \leq 0$$

## 2.3. Model Analysis

### 2.3.1. Monotonicity Analysis, Constraint Activity and Redundancy

In order to check for well boundedness, monotonicity analysis was performed on the optimization problem. Initially, a few variables were found to be unconstrained from below. This resulted in the addition of more constraints which resulted in a total of 21 constraints for 10 variables.

As can be seen from Table 2.4 below, the problem is well bounded and three constraints can be readily recognized as being active. However, since the number of active constraints does not equal the number of variables, the optimization problem can only be simplified but not solved by monotonicity analysis.

It can also be inferred from the table that one of the constraints $g_{14}$, $g_{15}$, $g_{16}$, $g_{17}$, $g_{18}$ or $g_{19}$ need to be active wrt d; one of $g_{11}$ or $g_{12}$ need to be a

ctive wrt $h_s$; $g_{18}$ or $g_{19}$ for $h_t$; $g_4$ or $g_6$ for $b_g$ and one of $g_1$ or $g_2$ need to be active wrt $d_r$. This can be examined at the end of optimization to validate the optimization routine.

### 2.3.2. Model Transformation

Of the 21 constraints, one (#10) is an equality constraint. In order to avoid any numerical rounding or termination error that may occur in the optimization routine, this constraint was explicitly solved for tan($\boldsymbol{\gamma_r}$). This resulted in the elimination of $\boldsymbol{\gamma_r}$ from the routine. The changed objective function and constraints are given below.

$$\tan\gamma_r = \frac{S_e - 1.05h_s}{b_r}$$

$$\text{Min V} = 1.05\,\frac{\pi d^2 h_s}{4} + l_t b_t h_t + b_r(S_e - 1.05h_s)t_r + l_g b_g h_g - b_r d_r h_g$$

$$\underbrace{h_g + (S_e - 1.05h_s) - h_s \le 0}_{g_{12}} \qquad \underbrace{\mu_r - \frac{S_e - 1.05h_s}{b_r} \le 0}_{g_{13}} \qquad \underbrace{\frac{k_\varphi(\emptyset_g - \emptyset_{k0})}{\frac{1}{2}d_r}\,\frac{1+\mu_r\frac{S_e-1.05h_s}{b_r}}{\frac{S_e-1.05h_s}{b_r}-\mu_r} - F_{appe} \le 0}_{g_{20}}$$

**Table 2.4 Monotonicity Analysis**

| | $d$ | $h_s$ | $l_t$ | $b_t$ | $h_t$ | $b_r$ | $\gamma_r$ | $l_g$ | $b_g$ | $d_r$ | Result |
|---|---|---|---|---|---|---|---|---|---|---|---|
| **f** | + | **U** | + | + | + | **U** | + | + | + | - | |
| **$g_1$** | | | - | | | | | | | + | **Active wrt $l_t$ by MPI** |
| **$g_2$** | | | | | | | | - | | + | **Active wrt $l_g$, by MPI** |
| **$g_3$** | | | | + | | - | | | | | |
| **$g_4$** | | | | | | + | | | - | | |
| **$g_5$** | | | | + | | | | | | - | |
| **$g_6$** | | | + | | | | | | - | | |
| **$g_7$** | + | | | - | | | | | | | **Active wrt $b_t$ by MPI** |
| **$g_8$** | | | + | | | - | | | | | |
| **$g_9$** | + | | | | | | | | | - | |
| **$g_{11}$** | | - | | | | | | | | | |
| **$g_{12}$** | | - | | | | + | + | | | | |
| **$g_{13}$** | | | | | | | - | | | | |
| **$g_{14}$** | - | | | | | | | | | | |
| **$g_{15}$** | - | + | | | + | | | | | | |
| **$g_{16}$** | - | | | | | | | | | | |
| **$g_{17}$** | - | + | | | | | | | | | |
| **$g_{18}$** | - | | | | - | | | | | | |
| **$g_{19}$** | - | | + | | - | | | | | | |
| **$g_{20}$** | | | | | | | **U** | | | - | |
| **$g_{21}$** | | | + | | | | | | | + | |

## 2.4. Optimization Study

### 2.4.1. Numerical Results

The above optimization problem with now 9 variables and 20 constraints was configured as an optimization problem using the software iSIGHT FD 3.1. The NLPQL algorithm was used with a step size of 1e-4 and a maximum of 100 iterations. Lower bound of 3 mm was assigned to all the variables. Plots of the objective function against the design variables is shown in Fig. 2.3. The objective is continuous in the design space and fairly monotonic (except with respect to x2 and x6 as predicted). A comparison of the starting points and the objective function can be found in Table 2.4. The active constraints are highlighted in green. The net volume of the latch was decreased by 20%.

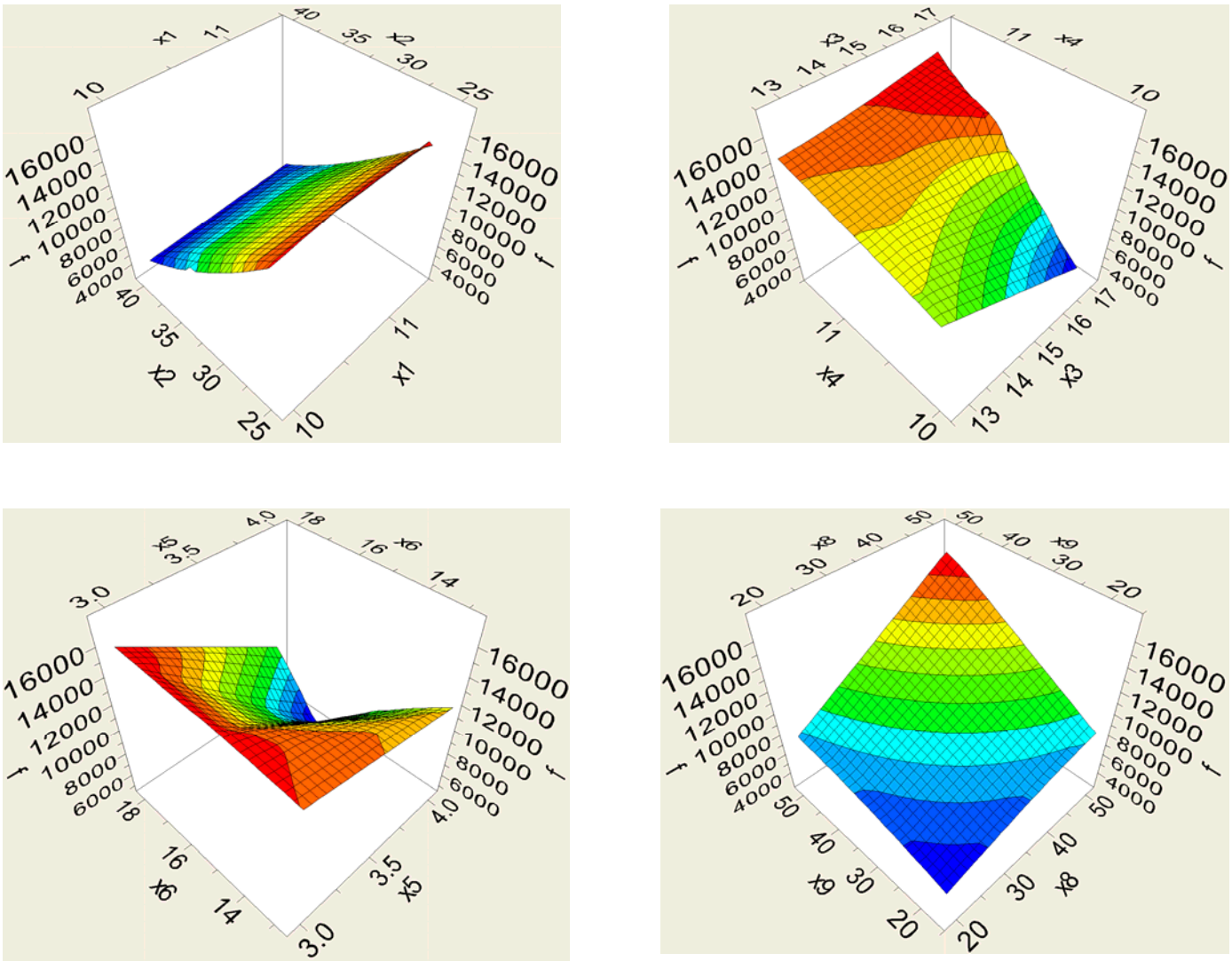

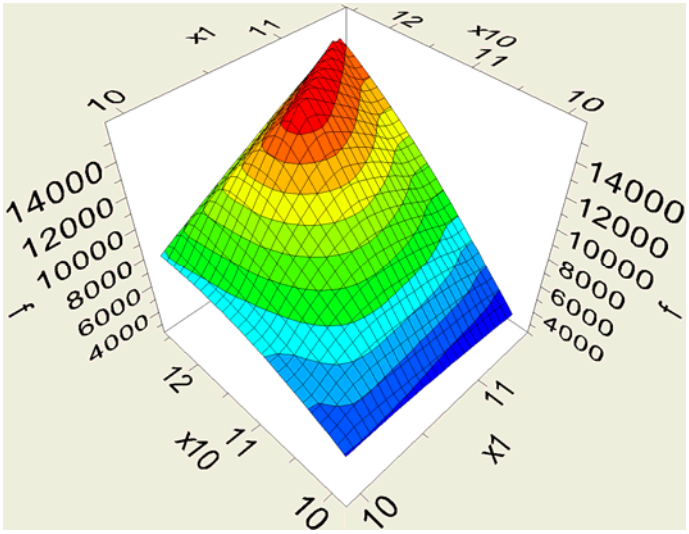


**Fig. 2.3 Plots showing variation of Objective Function with respect to the variables**

### 2.4.2. Monotonicity Analysis and Constraint Activity

Table 2.5 shows the comparison between the expected active constraints from monotonicity analysis and the actually active constraints after running the optimization routine. Clearly numerical results agree well with the monotonicity analysis. While running the program it was noticed that x5 hit its lower bound of 3 mm. So, it is considered as a parameter henceforth.

**Table 2.5 Crosscheck with Monotonicity Analysis**

| Variable | Expected Active Constraints | Resulting Active Constraints |
|---|---|---|
| $x_1$ | $g_{14}/g_{15}/g_{16}/g_{17}/g_{18}/g_{19}$ | $g_{15}$ |
| $x_2$ | $U$ | $g_{11}$ |
| $x_3$ | $g_1$ | $g_1$ |
| $x_4$ | $g_7$ | $g_7$ |
| $x_6$ | $U$ | $g_8$ |
| $x_8$ | $g2$ | $g_2$ |
| $x_9$ | $g_4/g_6$ | $g_4$ |
| $x_{10}$ | $g_1/g_2/g_{21}$ | $g_1/g_2$ |

**Table 2.6 Results from *iSIGHT***

| | Initial Values | iSIGHT Values |
|---|---|---|
| $x_1$ (mm) | 11.60 | 11.45 |
| $x_2$ (mm) | 26.00 | 26.00 |
| $x_3$ (mm) | 13.60 | 12.59 |
| $x_4$ (mm) | 13.00 | 11.45 |
| $x_5$ (mm) | 4.00 | 3.00 |
| $x_6$ (mm) | 13.60 | 12.59 |
| $x_7$ (deg) | 29.52 | 31.45 |
| $x_8$ (mm) | 60.00 | 51.91 |
| $x_9$ (mm) | 50.00 | 45.31 |
| $x_{10}$ (mm) | 13.60 | 12.59 |
| $g_1$ | 0.00 | 0.00 |
| $g_2$ | -6.98 | 0.00 |
| $g_3$ | -0.60 | -1.14 |
| $g_4$ | -3.58 | 0.00 |
| $g_5$ | -0.60 | -1.14 |
| $g_6$ | -36.40 | -32.72 |
| $g_7$ | -1.40 | 0.00 |
| $g_8$ | 0.00 | 0.00 |
| $g_9$ | -0.84 | 0.00 |
| $g_{10}$ | 0.00 | 0.00 |
| $g_{11}$ | 0.00 | 0.00 |
| $g_{12}$ | -13.30 | -13.30 |
| $g_{13}$ | -0.07 | -0.11 |
| $g_{14}$ | -622.42 | -620.33 |
| $g_{15}$ | -4.30 | 0.00 |
| $g_{16}$ | -639.93 | -638.31 |
| $g_{17}$ | -331.51 | -316.79 |
| $g_{18}$ | -308.22 | -293.54 |
| $g_{19}$ | -679.11 | -678.46 |
| $g_{20}$ | -16.57 | -79.09 |
| $g_{21}$ | -0.98 | -2.17 |
| ***V*** ***(mm$^3$)*** | ***1.7982e4*** | ***1.4499e4*** |

### 2.4.3. Karush-Kuhn-Tucker (KKT) Conditions

The KKT conditions can be described as-

$$\nabla f + \boldsymbol{\lambda^T} \nabla \boldsymbol{h} + \boldsymbol{\mu}^T \nabla \boldsymbol{g} = \mathbf{0}^T$$

$$\boldsymbol{h} = \mathbf{0}, \qquad \boldsymbol{g} \leq \mathbf{0}$$

$$\boldsymbol{\lambda} \neq \mathbf{0}, \ \boldsymbol{\mu} \geq \mathbf{0}, \ \boldsymbol{\mu}^T \boldsymbol{g} = \mathbf{0}$$

where f is the objective function,

**h** is the set of equality constraints,

**g** is the set of inequality constraints,

**λ** is the set of Lagrange Multipliers for equality constraints, and

**μ** is the set of Lagrange Multipliers for the inequality constraints

For the problem at hand, the inequality constraint has been explicitly solved and hence h would represent a null set. The number of variables is 8 (after excluding x5 and x7 for reasons stated before) and the number of inequality constraints is 20. From the result it is clear that there are 7 constraints (g1, g2, g4, g7, g8, g11 and g15) expected to be active. KKT analysis is performed to check the values of the multipliers corresponding to these active constraints.

To proceed with the KKT condition analysis, the vector $\mu^T$ needs to be defined. Since we know that g1, g2, g4, g7, g8, g11 and g15 appear to be active, we can set the multipliers of all other constraints to zero. The resultant vector is-

$$\boldsymbol{\mu} = [\mu_1, \mu_2, 0, \mu_4, 0, 0, \mu_7, \mu_8, 0, \ \mu_{11}, 0, 0, 0, \mu_{15}, 0, 0, 0, 0, 0, 0]^{\ T}$$

At the calculated optimal point, the gradient of the objective function was evaluated as follows-

$$\nabla f = [494, \quad 70.34, \quad 34.35, \quad 37.77, \quad -39.85, \quad 226.55, \quad 259.55, \quad -62.95]^T$$

The gradient of the inequality constraints was evaluated as-

$$\nabla \mathbf{g} = \begin{pmatrix}
0.00 & 0.00 & -1.00 & 0.00 & 0.00 & 0.00 & 0.00 & 1.00 \\
0.00 & 0.00 & 0.00 & 0.00 & 0.00 & -1.00 & 0.00 & 1.10 \\
0.00 & 0.00 & 0.00 & 1.00 & -1.00 & 0.00 & 0.00 & 0.00 \\
0.00 & 0.00 & 0.00 & 0.00 & 1.10 & 0.00 & -1.00 & 0.00 \\
0.00 & 0.00 & 0.00 & 1.00 & 0.00 & 0.00 & 0.00 & -1.00 \\
0.00 & 0.00 & 1.00 & 0.00 & 0.00 & 0.00 & -1.00 & 0.00 \\
1.00 & 0.00 & 0.00 & -1.00 & 0.00 & 0.00 & 0.00 & 0.00 \\
0.00 & 0.00 & 1.00 & 0.00 & -1.00 & 0.00 & 0.00 & 0.00 \\
1.10 & 0.00 & 0.00 & 0.00 & 0.00 & 0.00 & 0.00 & -1.00 \\
0.00 & -1.00 & 0.00 & 0.00 & 0.00 & 0.00 & 0.00 & 0.00 \\
0.00 & -2.05 & 0.00 & 0.00 & 0.00 & 0.00 & 0.00 & 0.00 \\
0.00 & 1.05 & 0.00 & 0.00 & 0.01 & 0.00 & 0.00 & 0.00 \\
-13.53 & 0.00 & 0.00 & 0.00 & 0.00 & 0.00 & 0.00 & 0.00 \\
-177.89 & 23.62 & 0.00 & 0.00 & 0.00 & 0.00 & 0.00 & 0.00 \\
-10.54 & 0.00 & 0.00 & 0.00 & 0.00 & 0.00 & 0.00 & 0.00 \\
-94.92 & 16.59 & 0.00 & 0.00 & 0.00 & 0.00 & 0.00 & 0.00 \\
-4.87 & 0.00 & 0.00 & 0.00 & 0.00 & 0.00 & 0.00 & 0.00 \\
-20.40 & 0.00 & 18.67 & 0.00 & 0.00 & 0.00 & 0.00 & 0.00 \\
0.00 & 83.77 & 0.00 & 0.00 & 48.80 & 0.00 & 0.00 & -9.30 \\
0.00 & 0.00 & 0.59 & 0.00 & 0.00 & 0.00 & 0.00 & 0.59
\end{pmatrix}$$

Using the sufficiency condition for an optimization problem with only inequality constraints $\nabla f + \boldsymbol{\mu}^T \nabla \boldsymbol{g} = \mathbf{0}^T$, the Lagrange Multipliers were calculated. These values were compared with the values as displayed by iSIGHT. A good agreement (except for $\mu_{11}$) was obtained. The result is summarized in Table 2.7.

Since the multipliers of the anticipated active constraints are all greater than zero, it can be concluded that the values of the design variables form a KKT point. Second order sufficiency is necessary to prove a minima but this would involve rigorous math. It can be stated that since the Lagrange Multipliers of the anticipated active constraints obtained at the design optimum are all greater than zero, the optimum is regular and is a KKT point. The global minimum is proved using non-gradient algorithms as shown in the next section.

**Table 2.7 Comparison of the values of Lagrange Multipliers**

| Multiplier | Calculated Values | iSIGHT Values |
|---|---|---|
| $\mu_1$ | 280.01 | 280.00 |
| $\mu_2$ | 226.55 | 226.55 |
| $\mu_4$ | 259.55 | 259.54 |
| $\mu_7$ | 37.77 | 37.77 |
| $\mu_8$ | 245.66 | 245.65 |
| $\mu_{11}$ | 157.33 | 205.62 |
| $\mu_{15}$ | 5.60 | 5.69 |

### 2.4.4. Other Observations

The starting point in the optimization routine was varied with respect to all the design variables. It was found that all the starting points converged to the same result. Although, this is not a sufficient condition to prove a global minimum, it gave more confidence of having found global optima. This also provided a check on the numerical stability of the routine.

It can also be seen that the active constraints bound all the design variables and hence, it can be said that solution was found on the boundary. Since the Hessian of the Lagrangian was too rigorous to calculate, Adaptive Simulated Annealing (ASA), a non-gradient algorithm, with a large number of iterations, was used. The optimum found from this algorithm was identical to the one obtained using the SQP algorithm. Thus it can be stated that the values of the variables and objective function given in Table 2.6 correspond to the global minima.

## 2.5. Parametric Study

The design of the T-Latch is inherently linked to the SMA sub-system. So, it would be interesting to study how the parameters like $F_{sma}$ and wrap diameter affect the objective function.

### 2.5.1. SMA force

The variation of the net volume of the latch with the force of SMA wire is show in Table 2.8. It is noted that $F_{sma}$ appears in a constraint that is not active. So $F_{sma}$ only defines the feasible region and when it remains within limits, it will not affect the objective function. This is observed from the table where for values of $F_{sma}$ about 22 N, the value of net volume of packaging remains constant. However, at about 19 N infeasible solutions are obtained. This shows that a very narrow feasible domain exists with respect to the force of the SMA wire. A minimum force of 22 N assumed as a parameter, however, would be valid.

### 2.5.2. Wrap Diameter

The wrap diameter also figures in an inactive constraint. Therefore, while it will not affect the objective function when it is within a range, outside this range, it will have an influence on the design variables and hence the objective function. Like the SMA force, the range is very narrow on one side of the presently assumed value of 12.7 mm. This is shown in Table 2.8.

### 2.5.3. Spring (Seal) Force

It was has been shown that several constraints containing parameters pertaining to the seal spring strongly influence the objective function. So it would indeed be interesting to see how the objective changes with the spring force. The range of the spring force, overall length, compressed length and outer diameter was obtained from the McMaster-Carr catalogue. The results are shown in Table 2.8.

**Table 2.8 Parametric Study**

| | Parameter | (1) | (2) | (3) | (4) | (5) |
|---|---|---|---|---|---|---|
| $F_{sma}$ | $F_{sma}$ | 19 | 20 | 21 | 22 | 24 |
| | V | Infeasible | 14499 | 14499 | 14499 | 14499 |
| $d_{wrap}$ | d_wrap | 11 | 12 | 12.7 | 14 | 20 |
| | V | Infeasible | 14499 | 14499 | 14499 | 14499 |
| Spring | $F_{sf}$ | 50 | 75 | 100 | 150 | 200 |
| | $S_e$ | 24.6 | 35 | 22.22 | 31.75 | 31.75 |
| | $S_c$ | 18 | 26 | 15 | 20.32 | 18.3 |
| | $S_d$ | 12.7 | 14.3 | 22.22 | 17.5 | 33.34 |
| | V | Infeasible | 14499 | 21572 | Infeasible | Infeasible |

It can be seen that the spring parameters strongly influence the variables and feasibility of the objective function. Care must be taken with this regard while designing the system. Since the wrap diameter and SMA force are strongly related to the second sub-system, this could be a matter of concern since a lot of infeasible points can be obtained during optimization. This could either imply an infeasible solution or a long optimization routine.

## 2.6. Discussion of Results

Numerical and analytical results using monotonicity analysis and the KKT conditions indicate that the optimum obtained is indeed a stationary point and could be global. The optimal solution gives a volume of about 15 $cm^3$. This makes physical sense as one can picture a device built to this overall dimension. The dimensions of the device mentioned in [1] support this statement. In the optimized dimensions, the volume of the latch was decreased by about 20%.

It is noted that most of the active constraints are practical constraints. This means that the design is determined more by geometry rather than stress limitations. That is, given precise manufacturing methods to attain smaller dimensions and given springs of desired dimensions, one could further reduce the net volume of the device while not violating the stress constraints. So, if there is a way, for example, to reduce the spring length and outer diameter while still maintaining the required seal force, a better solution can be obtained.

The tolerance on the designs to accommodate assembly misalignments, 10% of the base for example, was only an estimate. However, it strongly influences the constraints (active $g_2$ and $g_4$ for example). The tolerance could be reduced or increased depending on the availability of precise assembly or packaging space. This mimics the physical design process where parts are built to dimensions that tolerate small variations in assembly.

As noted in the parametric study, the tolerance of the feasibility of this subsystem relative to the variables of the second sub-system namely the SMA Force and the wrap diameter is very poor. This could dictate the feasible domain of the design in the system integration model. On the flip side, the shoulder length and the ramp spacing are parameters for the second subsystem. Depending on whether the constraints involved in that system are active or not, these could influence the system optima. This means that the two subsystems are essentially coupled and neither gets preference over the other while running the system optimization routine.

## 3. Spool-Packaged SMA Wire Actuator (Subsystem 2) : *WonHee Kim*

Shape Memory Alloy actuators are very attractive for many applications because of their high energy density, reduced size and weight, robust performance, and simple architecture. Especially SMA wire is more advantageous to be implemented because of its well-developed manufacturing and quality control, actuation with simple electrical control circuit, and fast heating and cooling speed. However, to ensure the enough strokes for a practical application, long lengths of SMA wire should be stored in a small package. To address this packaging challenge, a spooling technique that wraps portions of the wire around mandrels to reduce the packaged length had been used in applications such as active latches [1], pedestrian protection [3], vibration suppression in hand-held arms [4], and biomedical applications [5, 6]. But, this technique does sacrifice some performance due to accumulating friction between the SMA wire and mandrel. To understand the output motion and limitation of this technique, an analytical model for linear spooled SMA actuators had been studied by Redmond et al. [2, 7, 8]. In this study, we will use this analytical model to optimize the design of the SMA wire actuator.

### 3.1. Problem Statement

The performance of the spooled SMA is the function of its geometric and frictional parameters, SMA material properties, and the externally applied load. Fig. 3.1 shows these factors related to the actuator stroke.

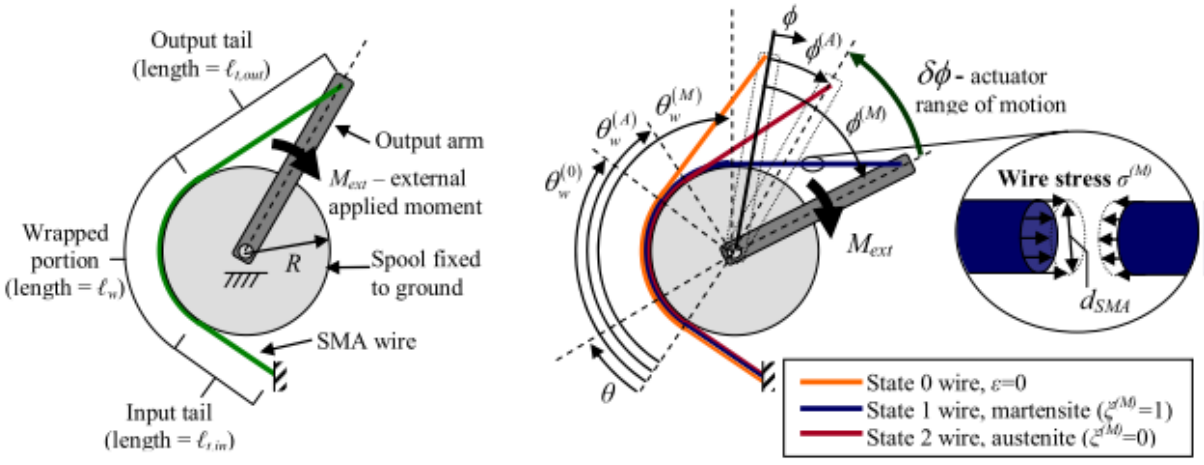


**Fig. 3.1 General architecture for spooled SMA actuators [8]**

Because of the non-linear behavior of the SMA wire, the performance of the SMA wire actuator is not linearly proportional to the geometry of the SMA wire actuator design, the diameter, length, and the free clearance, even with the straight wire actuator without spooling mechanism. With the spooling mechanism, there are more factors which affect the performance of the SMA wire actuator; such as the diameter of the spool, wrap angle, and the length of the input tail. The goal of this study is to optimize the spool-packaged SMA wire actuator design for the minimum input power usage.

## 3.2. Mathematical Model

### 3.2.1. Objective function

As mentioned in the problem statement, the object of this study is to minimize the input power for the phase transformation of the SMA wire from the martensite phase to the austenite phase, and the input power is determined by the diameter of the SMA wire $d_{SMA}$ and the total length of the SMA wire $\ell_{total}$.

$$f(\boldsymbol{x}) = \underbrace{\ell_{total} \times 2.527 \times 10^{-6} \times \left(\frac{d_{SMA}}{1000}\right)^{-1.946}}_{\text{R}} \times \underbrace{\left\{5.519 \times 10^{3} \times \left(\frac{d_{SMA}}{1000}\right)^{1.858}\right\}^{2}}_{\text{I}^2} \quad (3.1)$$

### 3.2.2. Constraints

The SMA wire actuator should generate the enough force to release the T-latch, and the required force is determined by the stiffness of the reset spring and the friction between the T of the latch and the engagement ramp.

$$F_{SMA}\{\phi_g, \xi^{(M)} = 0\} \geq \frac{k_\phi(\phi_g - \phi_{k0}) + \mu_g F_{SF}\frac{(\ell_T + d_r)}{4}}{d_{wrap}} \quad (3.2)$$

The stroke of the SMA wire actuator should be bigger than the required stroke which can release the T from the engagement ramp. And this stroke should be translated to the rotation.

$$\delta\phi = \theta_w^{(M)} - \theta_w^{(A)} \geq \phi_g \quad (3.3)$$

The force of the SMA wire can be calculated by the stress of the SMA wire and the cross

sectional area of the wire. The stress of the wire can be obtained by the constitutive model of the stress-strain relationship of the wire.

$$F_{SMA}\{\phi_g, \xi^{(M)} = 0\} = \sigma_{SMA}\{\varepsilon\{\phi_g\}, \xi^{(M)} = 0\}\left(\frac{1}{4}\pi d_{SMA}^2\right) \tag{3.4}$$

Without the spooling mechanism, the stroke of the SMA wire can be obtained by the changes of the equilibrium state between the SMA wire and the reset spring. And the equilibrium state can be obtained graphically with the constitutive model of the stress-strain curve. The stroke can be calculated by multiplying the original length with the difference between the austenite strain and the martensite strain. However, because of the friction between the SMA wire and the spool, we need to use the modification of the strain. Fig. 3.2 shows the effect of the friction in a differential element.

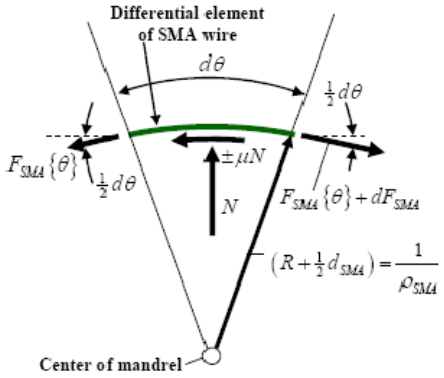


**Fig. 3.2 Free body diagram of a differential element of SMA in sliding contact with the spool [2]**

Equation (3.5) and (3.6) are the model of the stress at the angle $\theta$ under the martensite and the austenite respectively.

$$\sigma^{(M)}\{\theta\} = \sigma_{tail}^{(M)} e^{\mu_{SMA}\left(\theta-\theta_w^{(M)}\right)} \tag{3.5}$$

$$\sigma^{(A)}\{\theta\} = \sigma_{tail}^{(A)} e^{-\mu_{SMA}\left(\theta-\theta_w^{(A)}\right)} \tag{3.6}$$

As the strain of the SMA wire under the certain stress can be obtained by the constitutive model of the stress-strain relationship, we can get the modified strain with the equation (3.7) and (3.8).

$$\varepsilon^{(M)}\left\{\sigma^{(M)}\{\theta\}\right\} = f_{SMA}^{(M)}\left\{\sigma_{tail}^{(M)} e^{\mu_{SMA}\left(\theta-\theta_w^{(M)}\right)}\right\} \tag{3.7}$$

$$\varepsilon^{(A)}\left\{\sigma^{(A)}\{\theta\}\right\} = f_{SMA}^{(M)}\left\{\sigma_{tail}^{(A)} e^{\mu_{SMA}\left(\theta-\theta_w^{(A)}\right)}\right\} \tag{3.8}$$

Stress at the tail is determined by the counter force from the T-Latch.

$$\frac{k_\phi\left(\phi_g-\phi_{k0}\right)+\mu_g F_{SF}\frac{\left(\ell_T+d_r\right)}{4}}{d_{wrap}} = \sigma_{tail}^{(A)}\left(\frac{1}{4}\pi d_{SMA}^2\right) \tag{3.9}$$

$$\frac{\mu_g F_{SF}\frac{\left(\ell_T+d_r\right)}{4}}{d_{wrap}} = \sigma_{tail}^{(M)}\left(\frac{1}{4}\pi d_{SMA}^2\right) \tag{3.10}$$

Relating the un-deformed length of each half of the SMA wire to the strain profiles of the martensite and austenite wires yields the compatibility equations for each state.

$$\ell_{total}^{(0)} = \int_0^{\theta_w^{(M)}}\left[1+f_{SMA}^{(M)}\left\{\sigma_{tail}e^{\mu_{SMA}\left(\theta-\theta_w^{(M)}\right)}\right\}\right]^{-1} d\theta + \frac{\ell_{tail}}{1+f_{SMA}^{(M)}\{\sigma_{tail}\}} \tag{3.11}$$

$$\ell_{total}^{(0)} = \int_0^{\theta_w^{(A)}}\left[1+f_{SMA}^{(A)}\left\{\sigma_{tail}e^{-\mu_{SMA}\left(\theta-\theta_w^{(A)}\right)}\right\}\right]^{-1} d\theta + \frac{\ell_{tail}}{1+f_{SMA}^{(A)}\{\sigma_{tail}\}} \tag{3.12}$$

The constitutive model of the stress-strain of the SMA wire can be obtained from the experiment data by curve fitting. We will use the constitutive model of the previous study [8].

$$\sigma^{(M)} = 4.6\times10^6\varepsilon^3 - 3.0\times10^5\varepsilon^2 + 6.8\times10^3\varepsilon + 21.4 \tag{3.13}$$

$$\sigma^{(A)} = 72.5\times10^3\varepsilon \tag{3.14}$$

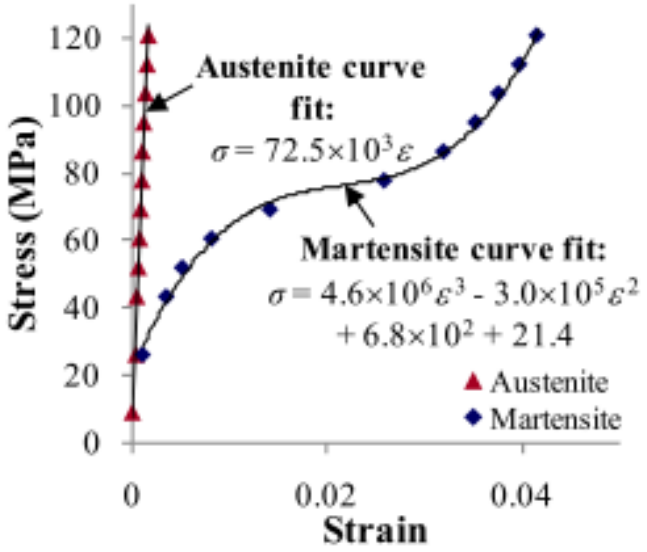


**Fig. 3.3 Stress-strain model for material behavior [8]**

One of the limitations of the SMA is that it shows the shakedown effect. To avoid the shakedown effect of the SMA wire actuator, the maximum stress should be limited within 250MPa ($\sigma_{SMA}$), and the maximum strain should be less than 4% [9].

$$\sigma_{SMA}\{\varepsilon\{\phi_g\}, \xi^{(M)} = 0\} \leq \sigma_{SMA} \quad 3.15)$$

$$\varepsilon^{(A)}\left\{\sigma^{(A)}\{\theta\}\right\} = f_{SMA}^{(M)}\left\{\sigma_{tail}^{(A)} e^{\mu_{SMA}\left(\theta-\theta_w^{(A)}\right)}\right\} \leq 0.04 \quad (3.16)$$

To connect the SMA wire to the spool, minimum length of the wrap length should be ensured. In addition to the minimum length of the wrap length, the tail length must be smaller than the total length of the SMA wire. To ensure these conditions, instead of the tail length we can introduce the ratio between the tail length and the total length.

$$\ell_{ratio} = \frac{\ell_{tail}}{\ell_{total}} \quad (3.17)$$

$$0 < \ell_{ratio} \leq 0.7 \quad (3.18)$$

The SMA wire is available as a commercial product with the 6, 8, 10, 12, 15, and 20 mil. For the optimization study, we will consider the diameter of the SMA wire as a continuous variable.

$$6 \leq d_{SMA} \leq 20 \quad (3.19)$$

The diameter of the spool should be bigger than the diameter of the shaft.

$$10 \leq d_{wrap} \quad (3.20)$$

### 3.2.3. Design Variables and Parameters

#### 3.2.3.1. Design Variables (Table 3.1)

| No. | Symbol | Description | Unit | Feasible Value |
|---|---|---|---|---|
| 1 | $d_{wrap}$ | diameter of spool | mm | 12.7 mm |
| 2 | $d_{SMA}$ | diameter of SMA wire | mil | 15 mil |
| 3 | $\ell_{total}$ | total length of the SMA wire | mm | 150 mm |
| 4 | $\ell_{ratio}$ | tail length / total length | | 0.66 |

3.2.3.2. Design Parameters (Table 3.2)

| No. | Symbol | Description | Value |
|---|---|---|---|
| 1 | $\phi_g$ | angle of engagement between the T and the ramp | 30º |
| 2 | $\phi_{k0}$ | angle of the reset spring at the initial state | 0º |
| 3 | $\mu_g$ | friction coefficient between the T and the ramp | 0.4 |
| 4 | $\mu_{SMA}$ | friction coeff. between the SMA wire and the | 0.15 |
| 5 | $d_r$ | ramp spacing | 10 mm |
| 6 | $\ell_{\mathrm{T}}$ | shoulder length of the T | 16.75 mm |
| 7 | $F_{SF}$ | seal force of the T-Latch | 75 N |
| 8 | $k_\phi$ | stiffness of the reset spring | 2.1 N-mm/deg. |
| 9 | $\sigma_{shake,SMA}$ | stress limit of SMA wires to avoid shakedown | 250 MPa |

### 3.2.4. Summary Model

minimize $f(\boldsymbol{x}) = \underbrace{\ell_{total} \times 2.527 \times 10^{-6} \times \left(\frac{d_{SMA}}{1000}\right)^{-1.946}}_{} \times \underbrace{\left\{5.519 \times 10^{3} \times \left(\frac{d_{SMA}}{1000}\right)^{1.858}\right\}^{2}}_{}$

subject to

$$\mathrm{g}(1) = \frac{k_\phi(\phi_g - \phi_{k0}) + \mu_g F_{SF}\frac{(\ell_T + d_r)}{4}}{d_{wrap}} - \sigma_{SMA}\{\varepsilon\{\phi_g\}, \xi^{(M)} = 0\}\left(\frac{1}{4}\pi d_{SMA}^2\right) \le 0$$

$$\mathrm{g}(2) = \phi_g - \delta\phi = \phi_g - \theta_w^{(M)} - \theta_w^{(A)} \le 0$$

$$\mathrm{g}(3) = \sigma_{SMA}\{\varepsilon\{\phi_g\}, \xi^{(M)} = 0\} - \sigma_{shake,SMA} \le 0$$

$$\mathrm{g}(4) = \varepsilon^{(A)}\left\{\sigma^{(A)}\{\theta\}\right\} - 0.04 = f_{SMA}^{(M)}\left\{\sigma_{tail}^{(A)}\right\} - 0.04 \le 0$$

$$\mathrm{h}(1) = \ell_{total}^{(0)} - \int_0^{\theta_w^{(M)}}\left[1 + f_{SMA}^{(M)}\left\{\sigma_{tail}^{(M)} e^{\mu_{SMA}\left(\theta - \theta_w^{(M)}\right)}\right\}\right]^{-1} d\theta - \frac{\ell_{ratio} \times \ell_{total}}{1 + f_{SMA}^{(M)}\{\sigma_{tail}^{(M)}\}} = 0$$

$$\mathrm{h}(2) = \ell_{total}^{(0)} - \int_0^{\theta_w^{(A)}}\left[1 + f_{SMA}^{(A)}\left\{\sigma_{tail}^{(A)} e^{-\mu_{SMA}\left(\theta - \theta_w^{(A)}\right)}\right\}\right]^{-1} d\theta - \frac{\ell_{ratio} \times \ell_{total}}{1 + f_{SMA}^{(A)}\{\sigma_{tail}^{(A)}\}} = 0$$

$$\mathrm{h}(3) = \sigma^{(M)} - 4.6 \times 10^6 \varepsilon^3 + 3.0 \times 10^5 \varepsilon^2 - 6.8 \times 10^3 \varepsilon - 21.4 = 0$$

$$\mathrm{h}(4) = \sigma^{(A)} - 72.5 \times 10^3 \varepsilon = 0$$

$$\mathrm{h}(5) = \frac{k_\phi(\phi_g - \phi_{k0}) + \mu_g F_{SF}\frac{(\ell_T + d_r)}{4}}{d_{wrap}} - \sigma_{tail}^{(A)}\left(\frac{1}{4}\pi d_{SMA}^2\right) = 0$$

$$h(6) = \frac{\mu_g F_{SF} \frac{(\ell_T + d_r)}{4}}{d_{wrap}} - \sigma_{tail}^{(M)} \left(\frac{1}{4}\pi d_{SMA}^2\right) = 0$$

set constraints

$$0 < \ell_{ratio} \leq 0.7,\ 6 \leq d_{SMA} \leq 20,\ 10 \leq d_{wrap}$$

## 3.3. Model Analysis

The objective function of the model contains two design variables, and the function is monotonic with respect to both of them.

$$f\left(\ell_{total}{}^{+}, d_{SMA}{}^{+}\right)$$

The inequality constraint g(1) and the equality constraint h(5) are redundant constraints, and g(1) should be active constraint.

$\theta_w^{(M)}$ and $\theta_w^{(A)}$ can be calculated from the equality constraints h(1) and h(2) respectively.

$$\theta_w^{(M)} = f(\ell_{total}^{(0)}, \ell_{tail}, f_{SMA}^{(M)}, \sigma_{tail}^{(M)})$$

$$\theta_w^{(A)} = f(\ell_{total}^{(0)}, \ell_{tail}, f_{SMA}^{(A)}, \sigma_{tail}^{(A)})$$

The values of $\theta_w^{(M)}$ and $\theta_w^{(A)}$ are not monotonic with respect to the variables, so it is hard to do the monotonicity analysis with the inequality constraint g(2).

$f_{SMA}^{(M)}$ and $f_{SMA}^{(A)}$ are the inverse functions of the function h(3) and h(4), and $f_{SMA}^{(A)}$ is monotonic with respect to $\sigma_{tail}^{(A)}$. And $\sigma_{tail}^{(A)}$ is derived from the equality constraint h(5).

$$\sigma_{tail}^{(A)} = f(d_{wrap}{}^{+}, d_{SMA}{}^{-})$$

However, because of the relation between other variables, it is hard to predict the activity of g(4).

## 3.4. Optimization Study

### 3.4.1. Optimization Results

Just as stated in the section 3.4, the complexity the $\theta_w^{(M)}$ and $\theta_w^{(A)}$ makes this model very difficult to calculate. To address this problem, iSight-FD is used with MATLAB code with Sequential Quadratic Programming (SQP). To verify the results from the SQP, Simulated Annealing and the Genetic Algorithm also had been used.

The feasible values in Table 3.1 are used as the initial condition with the SQP method.

| No. | Symbol | Description | Unit | Feasible Value |
|---|---|---|---|---|
| 1 | $d_{wrap}$ | diameter of spool | mm | 12.7 mm |
| 2 | $d_{SMA}$ | diameter of SMA wire | mil | 15 mil |
| 3 | $\ell_{total}$ | total length of the SMA wire | mm | 150 mm |
| 4 | $\ell_{ratio}$ | tail length / total length | | 0.66 |

The value of *f(x)* with the initial condition is 6.825, and after 65 times of iteration, the possible local minima are obtained as Table 3.3 with the *f(x)* value 2.865.

**Table 3.3 Possible local minima**

| **Variables** | $d_{SMA}$ | $d_{wrap}$ | $\ell_{total}$ | $\ell_{ratio}$ | *f(x)* |
|---|---|---|---|---|---|
| **Value** | 14.95 mil | 10mm | 63.29mm | 0.7 | 2.865 |

The result of the optimization shows 58% of the improvement with the objective function value. To check the global convergence, model had been tested with the different starting points (Table 3.4).

**Table 3.4 Results with the different initial condition**

| **Initial Values** | | | | **Local Minima** | | | | |
|---|---|---|---|---|---|---|---|---|
| $d_{SMA}$ | $d_{wrap}$ | $\ell_{total}$ | $\ell_{ratio}$ | $d_{SMA}$ | $d_{wrap}$ | $\ell_{total}$ | $\ell_{ratio}$ | *f(x)* |
| 15 | 12.7 | 150 | 0.66 | 14.95 | 10 | 63.29 | 0.7 | 2.865 |
| 6 | 10 | 40 | 0 | 14.95 | 10 | 63.29 | 0.7 | 2.865 |
| 20 | 50 | 600 | 0.7 | - | - | - | - | - |

While the model converges to the same optimum point from the lower starting values, it did not find the optimum point with the upper bound values. Because of this non-convergence from the upper bound values, Simulated Annealing (SA) and Genetic Algorithm (GA) had been used to verify the results with the SQP (Table 3.5).

**Table 3.5 Results with the different initial condition**

| **Method** | $d_{SMA}$ | $d_{wrap}$ | $\ell_{total}$ | $\ell_{ratio}$ | *f(x)* |
|---|---|---|---|---|---|
| **SQP** | 14.95 mil | 10 mm | 63.29 mm | 0.7 | 2.865 |
| **SA** | 7.08 mil | 44.50 mm | 276.22 mm | 0.68 | 3.336 |
| **GA** | 7.51 mil | 40.63 mm | 284.00 mm | 0.51 | 3.190 |

These results show that the result with the SQP is the optimum point, but the problem with the global seems to be caused by the discontinuous feasible region and the non-monotonic relation between the actuation angle and the diameter and the length of wire (Figure 3.4). The diameter of the spool and the tail length ratio which are not included in the objective function show the non-monotonicity with the objective function value (Figure 3.5).

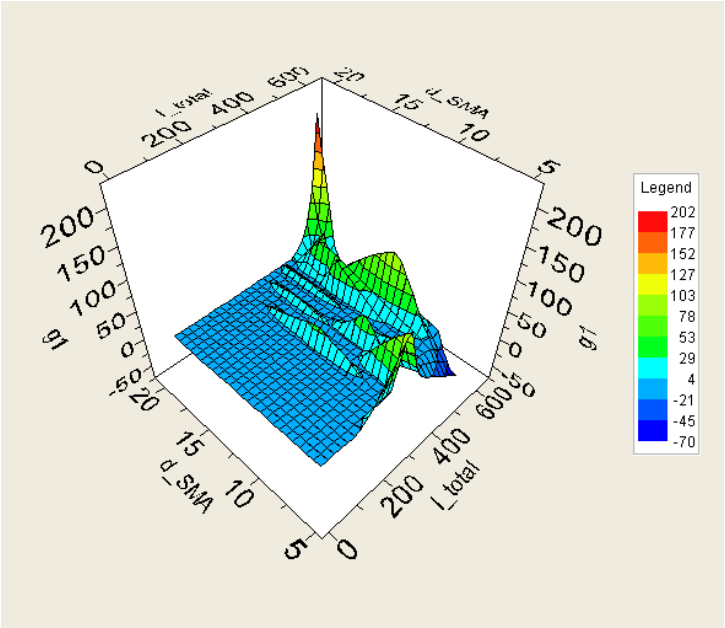


**Fig. 3.4 Actuation angle vs the SMA wire diameter and the length of the wire**

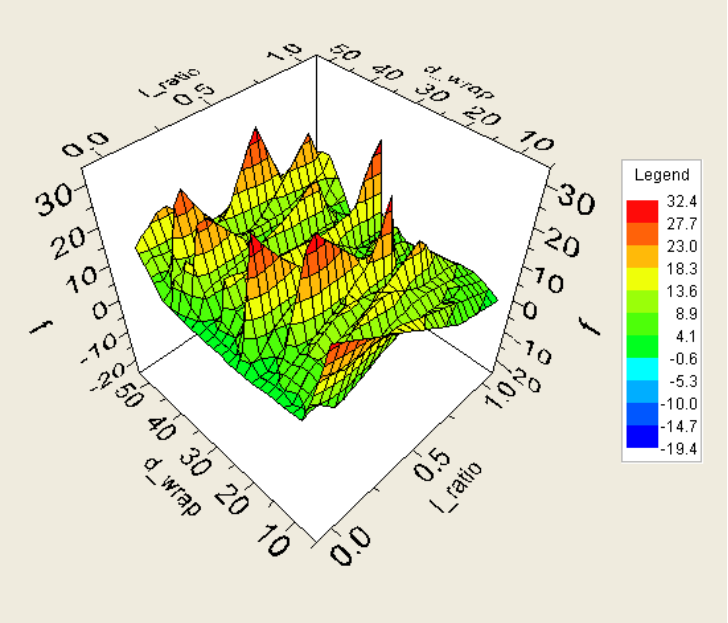


**Fig. 3.5 The objective function values vs the spool diameter and the tail length ratio**

### 3.4.2. Constraints Activity

At the optimum point we found, inequality constraints g(1) and g(3) are active. As stated in the model analysis g(1) should be always active with the equality constraint h(5).

$$g(1) = \frac{k_\phi(\phi_g - \phi_{k0}) + \mu_g F_{SF}\frac{(\ell_T + d_r)}{4}}{d_{wrap}} - \sigma_{SMA}\{\varepsilon\{\phi_g\}, \xi^{(M)} = 0\}\left(\frac{1}{4}\pi d_{SMA}^2\right) \le 0$$

$$g(3) = \sigma_{SMA}\{\varepsilon\{\phi_g\}, \xi^{(M)} = 0\} - \sigma_{shake,SMA} \le 0$$

These activities of the inequalities are about the stress on the SMA wire, and these are similar to the "full stress design" method. And the objective function only contains $d_{SMA}$, $\ell_{total}$, the optimizer tries to reduce the diameter of the SMA wire by increasing the diameter of the spool, but the increase of the SMA wire diameter also increases the length of the SMA wire. The set constraint of the spool diameter is active because of these relations.

$$\ell_{ratio} \le 0.7,\ 10 \le d_{wrap}$$

And the wrap portion of the SMA wire always decreases the actuation stroke (rotation of the spool) by the loss of the friction. So the $\ell_{ratio}$ is always tends to be increased.

## 3.5. Parametric Study

To check the effect of the parameters on the optimum point, some of the parameters, seal force of the T-Latch, actuation angle, and the limit stress of the SMA wire to avoid the shakedown, had been studied with the different values.

Table 3.7 shows the results with the different $F_{sf}$ values. And the changes in the $F_{sf}$ values initiate the changes in the diameter of the SMA wire. And the increase of the SMA wire diameter causes the decrease in the length of the SMA wire.

**Table 3.6 Parametric study on the seal force**

| $F_{sf}$ | $d_{SMA}$ | $d_{wrap}$ | $\ell_{total}$ | $\ell_{ratio}$ | f(x) |
|---|---|---|---|---|---|
| **50 N** | 12.92 mil | 10 mm | 66.07 mm | 0.7 | 2.308 |
| **75 N** | 14.95 mil | 10 mm | 63.29 mm | 0.7 | 2.865 |
| **100 N** | 16.75 mil | 10 mm | 62.23 mm | 0.7 | 3.440 |
| **125 N** | 18.36 mil | 10 mm | 61.58 mm | 0.7 | 4.008 |
| **150 N** | 19.84 mil | 10 mm | 61.20 mm | 0.7 | 4.571 |

Table 3.7 and 3.8 are the results with the different actuation angles and the stress limits respectively.

**Table 3.7 Parametric study on the actuation angle**

| $\delta\phi$ | $d_{SMA}$ | $d_{wrap}$ | $\ell_{total}$ | $\ell_{ratio}$ | f(x) |
|---|---|---|---|---|---|
| **20°** | 14.95 mil | 10 mm | 41.36 mm | 0.7 | 1.870 |
| **25°** | 14.95 mil | 10 mm | 52.21 mm | 0.7 | 2.364 |
| **30°** | 14.95 mil | 10 mm | 63.29 mm | 0.7 | 2.865 |
| **35°** | 14.95 mil | 10 mm | 74.67 mm | 0.7 | 3.380 |
| **40°** | 14.95 mil | 10 mm | 86.48 mm | 0.7 | 3.915 |
| **45°** | 14.95 mil | 10 mm | 98.75 mm | 0.7 | 4.470 |

**Table 3.8 Parametric study on the limit stress of the SMA wire to avoid shakedown**

| $\sigma_{shake,SMA}$ | $d_{SMA}$ | $d_{wrap}$ | $\ell_{total}$ | $\ell_{ratio}$ | f(x) |
|---|---|---|---|---|---|
| **100 MPa** | 20 mil | 13.98 mm | 160.01 mm | 0.7 | 12.11 |
| **150 MPa** | 19.31 mil | 10 mm | 79.17 mm | 0.7 | 5.630 |
| **200 MPa** | 16.72 mil | 10 mm | 68.58 mm | 0.7 | 3.780 |
| **250 MPa** | 14.95 mil | 10 mm | 63.29 mm | 0.7 | 2.865 |

These results shows the relations between the actuation angles and the length of the SMA wire, and the effect on the optimum design with the different stress limits. Most of them show the linear relations except for the limit stress with the 100MPa case.

## 3.6. Discussion of Results

As already stated in the constraints activity these results are physically meaningful. The diameter of the SMA wire is related to the limit stress of the SMA wire and the diameter of the spool under the same moment required releasing the T-Latch. As the value of the objective function can be decreased by reducing the diameter of the SMA wire, the SMA wire diameter is determined by the stress limit.

And the total length of the wire is determined by the actual stress on the SMA wire and the required actuation angle. As the spooling decreases the actuation stroke of the SMA wire by the friction, the wrap portion of the SMA wire tends to be decreased.

**Table 3.3 Optimum point**

| Variables | $d_{SMA}$ | $d_{wrap}$ | $\ell_{total}$ | $\ell_{ratio}$ | f(x) |
|---|---|---|---|---|---|
| **Value** | 14.95 mil | 10mm | 63.29mm | 0.7 | 2.865 |

Depends on the parameters of the model such as the seal force, the actuation angle, and the stress limit of the SMA wire, the optimum point can be changed. Particularly the stress limit can change the activity of the constraint. As the many of the active constraints are based on the design decision, they should be determined carefully.

# 4. System Integration Study

## 4.1. Mathematical Model

The wrap diameter and SMA force influence the feasibility of the latch design. The seal force and the actuation angle influence the feasibility of the spool design. So, the system consisting of the latch mechanism to be actuated by the spool, will indeed be a tradeoff between the two sub systems.

The objective function of the system is to reduce the footprint and hence the packaging volume of the whole device. The initial mini-max formulation was converted to a minimization problem by subjecting a part of the objective function as constraints. The overall system model is given below.

**Min** $V_p = max(d\_wrap + 2 * l\_total * l\_ratio, bg) * max(1.3 * max(d, d\_wrap), lg) * (hs + hw + hg)$

**Subject to**

1. $d_r - l_t \leq 0$
2. $1.1\,(d_r + 2t_r + 2S_d) - l_g \leq 0$
3. $b_t - b_r \leq 0$
4. $1.1\,(b_r + 2S_d) - b_g \leq 0$
5. $1.1\,b_t - d_r \leq 0$
6. $l_t - b_g \leq 0$
7. $d - b_t \leq 0$
8. $l_t - b_r \leq 0$
9. $1.1\,d - d_r \leq 0$
10. $1.05\,h_s + b_r\,tan(\gamma_r) - S_e = 0$
11. $S_c - h_s \leq 0$
12. $h_g + b_r\,tan(\gamma_r) - h_s \leq 0$

13. $\mu_r - \tan(\gamma_r) \leq 0$

14. $\sigma_E = \sqrt{\left\{\frac{F_{SF}}{\frac{1}{4}\pi d^2}\right\}^2 + 3\left\{\frac{16F_{app}}{3\pi d^2}\right\}^2} - S_y \leq 0$

15. $\sigma_F = \frac{32}{\pi}\frac{F_{appr}(h_s + h_t)}{d^3} + \frac{F_{SF}}{\frac{1}{4}\pi d^2} - S_y \leq 0$

16. $\sigma_A = \sqrt{\left\{\frac{F_{appr}\cos a + F_{SF}}{\frac{1}{4}\pi d^2}\right\}^2 + 3\left\{\frac{16}{3\pi}\frac{F_{appr}\sin a}{d^2}\right\}^2} - S_y \leq 0$

17. $\sigma_B = \frac{F_{appr}\cos a + F_{SF}}{\frac{1}{4}\pi d^2} + \frac{32}{\pi}\frac{F_{appr}\sin a\,(h_s - h_g)}{d^3} - S_y \leq 0$

18. $\zeta_C = \frac{3}{4}\frac{F_{appr}\cos a + F_{SF}}{d h_t} - \frac{S_y}{2} \leq 0$

19. $\sigma_D = \frac{3}{4}\frac{\left(F_{appr}\cos a + F_{SF}\right)\left(\frac{l_t}{d} - 1\right)}{{h_t}^2} - S_y \leq 0$

20. $\frac{k_\varphi\left(\emptyset_g - \emptyset_{k0}\right)}{\frac{1}{2}d_r}\frac{1 + \mu_r \tan\gamma_r}{\tan\gamma_r - \mu_r} - F_{appe} \leq 0$

21. $\frac{k_\phi\left(\phi_g - \phi_{k0}\right) + \mu_g F_{SF}\frac{(\ell_T + d_r)}{4}}{d_{wrap}} - \sigma_{SMA}\left\{\varepsilon\left\{\phi_g\right\}, \xi^{(M)} = 0\right\}\left(\frac{1}{4}\pi d_{SMA}^2\right) \leq 0$

22. $\phi_g - \delta\phi = \phi_g - \theta_w^{(M)} - \theta_w^{(A)} \leq 0$

23. $\sigma_{SMA}\left\{\varepsilon\left\{\phi_g\right\}, \xi^{(M)} = 0\right\} - \sigma_{shake,SMA} \leq 0$

24. $\varepsilon^{(A)}\left\{\sigma^{(A)}\{\theta\}\right\} - 0.04 = f_{SMA}^{(M)}\left\{\sigma_{tail}^{(A)}\right\} - 0.04 \leq 0$

25. $\ell_{total}^{(0)} - \int_0^{\theta_w^{(M)}}\left[1 + f_{SMA}^{(M)}\left\{\sigma_{tail}^{(M)} e^{\mu_{SMA}\left(\theta - \theta_w^{(M)}\right)}\right\}\right]^{-1} d\theta - \frac{\ell_{ratio}\times\ell_{total}}{1 + f_{SMA}^{(M)}\left\{\sigma_{tail}^{(M)}\right\}} = 0$

26. $\ell_{total}^{(0)} - \int_0^{\theta_w^{(A)}} \left[1 + f_{SMA}^{(A)} \left\{\sigma_{tail}^{(A)} e^{-\mu_{SMA}\left(\theta - \theta_w^{(A)}\right)}\right\}\right]^{-1} d\theta - \frac{\ell_{ratio} \times \ell_{total}}{1 + f_{SMA}^{(A)}\left\{\sigma_{tail}^{(A)}\right\}} = 0$

27. $\sigma^{(M)} - 4.6 \times 10^6 \varepsilon^3 + 3.0 \times 10^5 \varepsilon^2 - 6.8 \times 10^3 \varepsilon - 21.4 = 0$

28. $\sigma^{(A)} - 72.5 \times 10^3 \varepsilon = 0$

28. $\frac{k_\phi(\phi_g - \phi_{k0}) + \mu_g F_{SF} \frac{(\ell_T + d_r)}{4}}{d_{wrap}} - \sigma_{tail}^{(A)} \left(\frac{1}{4}\pi d_{SMA}^2\right) = 0$

30. $\frac{\mu_g F_{SF} \frac{(\ell_T + d_r)}{4}}{d_{wrap}} - \sigma_{tail}^{(M)} \left(\frac{1}{4}\pi d_{SMA}^2\right) = 0$

As the objective function of this integrated model has a comparison function (max), it may not be differentiable at some points. To address this problem, intermediate variables were introduced to find the largest lengths in the design. The resulting objective function is-

$$\min f = (m1 \times m2 \times (hs + 20 + 5))$$

where, *m1* and *m2* represent the largest lengths. To find the *m1* and *m2* value, new constraints were introduced.

$$d_{wrap} + (2 \times l_{total} \times l_{ratio}) - m1 \leq 0$$
$$bg - m1 \leq 0$$
$$d - m21 \leq 0$$
$$d_{wrap} - m21 \leq 0$$
$$m21 - m2 \leq 0$$
$$lg - m2 \leq 0$$

By using new intermediate variables and constraints, the problem with using non-differentiable function was addressed.

## 4.2. Numerical Results

The combined system model was run using iSIGHT with necessary modifications to the maximum number of iterations and step size to allow a smooth step to overcome any numerical noise generated by the integration of a few functions. The results from the subsystems had been used as the starting point for the combined system. The results are compared in Table 4.1.

**Table 4.1 Comparison of the results from the overall system and individual subsystems**

| Variable | System | Subsystem 1 | Subsystem 2 |
|---|---|---|---|
| *x1* (mm) | 11.45 | 11.45 | |
| *x2* (mm) | 26.00 | 26.00 | |
| *x3* (mm) | 12.59 | 12.59 | |
| *x4* (mm) | 11.45 | 11.45 | |
| *x5* (mm) | 3.00 | 3.00 | |
| *x6* (mm) | 12.74 | 12.59 | |
| *x7* (deg) | 31.45 | 31.45 | |
| *x8* (mm) | 51.91 | 51.91 | |
| *x9* (mm) | 45.47 | 45.31 | |
| *x10* (mm) | 12.59 | 12.59 | |
| $d_{SMA}$ (mil) | 15.00 | | 14.95 |
| $d\_{wrap}$ (mm) | 9.50 | | 10.00 |
| $\boldsymbol{\ell_{ratio}}$ | 0.48 | | 0.70 |
| $\boldsymbol{\ell_{total}}$ (mm) | 72.36 | | 63.29 |
| $f$ (mm$^3$) | 210934.60 | | |

To verify the result of the design, the different starting points and the different methods were used. Due to the non-monotonicity of the subsystem2, the results with the different starting points were different. Since we could not obtain results from non-gradient algorithms, a global optimum cannot be claimed.

## 4.3. Parametric Study

### 4.3.1. Spring Force

It would be interesting to see how the spring force, a parameter for both subsystems, would affect the design of the system. Also, the wire diameter, a design variable in subsystem 2 is a parameter in the system problem. A parametric study would show how this decision affects the system optimum.

As seen from Table 4.2, there is a very narrow feasible domain with respect to spring force. This is predictable since one of the constituent subsystems was very sensitive to variations in spring force.

**Table 4.2 Effect of Spring Force**

| Spring Force (N) | Objective Function ($mm^3$) |
|---|---|
| **50** | **210915** |
| **75** | **210935** |
| **100** | Infeasible |
| **125** | Infeasible |

### 4.3.2. SMA Wire Diameter

The wire diameter, a variable in Subsystem 2 was taken as a parameter in the integrated system model. So, a parametric study was performed on the different available wire diameters, the results of which are summarized in Table 4.3. It is clear that a narrow feasible range also applies to the wire diameter.

**Table 4.3 Effect of SMA Wire Diameter**

| Wire Diameter (mil) | Objective Function ($mm^3$) |
|---|---|
| **6** | Infeasible |
| **8** | Infeasible |
| **10** | Infeasible |
| **12** | Infeasible |
| **15** | **210935** |
| **20** | **142718** |

## 4.4. Discussion of Results

The result gives the volume of packaging of the device is greater than the net volume of the 'T' alone. This shows a strong correlation between the two subsystems. If the parameters of the subsystems could be dynamically changed as the system integration model changes, the individual subsystems would benefit.

More investigation is necessary to understand why the non-gradient based algorithms could not arrive at a feasible point even after a considerable amount of running time. In other words, the narrow feasible region of the problem remains to be analyzed.

The total footprint of the device is about 211 $cm^3$. This is the space under the hood of the car required to support the device.

## 5. Acknowledgments

We would like to thank the *Smart Materials and Structures* group at the University of Michigan, particularly Prof. Diann Brei and John A Redmond for their assistance in framing the optimization problem for both the subsystems. We are indebted to Kwang Jae Lee who was always ready to help us out with specific issues regarding modeling and using iSIGHT. We are grateful to Prof. Papalambros for his constant support throughout the span of the project. His foresight and inputs helped avert hours of troubleshooting.

## 6. References

[1] Redmond, J. A., Brei, D. E., Luntz, J., Browne, A. L., Johnson, N. L., and Strom, K. "Design and Experimental Validation of an Ultrafast SMART (Shape Memory Alloy ReseTtable) Latch", Proc. ASME, IMECE2007-43372 (2007).

[2] Redmond, J., Brei, D., Luntz, J., Browne, A., and Johnson, N. “Behavioral model and experimental validation for spool-packaged shape memory alloy linear actuators”, Proc. 19th International Conference on Adaptive Structures and Technologies (2008).

[3] Barnes, B., Brei, D., Luntz, J., Browne, A., and Strom, K. "Panel Deployment Using Ultrafast SMA Latches", Proc. ASME, IMECE2006-15026 (2006).

[4] Pathak, A., Brei, D., Luntz, J., LaVigna, C., and Kwatny, H. "Design and quasi-static characterization of SMASH: SMA stabilizing handgrip", Proc. SPIE 6523 (2007).

[5] Menciassi, A., Gorini, S., Moglia, A., Pernorio, G., Stefanini, C., and Dario, P. "Clamping Tools of a Capsule for Monitoring the Gastrointestinal Tract Problem Analysis and Preliminary Technological Activity." Proc. IEEE, Robotics and Automation, 1309-1314 (2005).

[6] Redmond, J., Brei, D., Luntz, J., Browne, A., and Johnson, N. "Behavioral model and experimental validation for spool-packaged shape memory alloy actuator", Proc. SPIE, 6930 (2008).

[7] Redmond, J., Brei, D., Luntz, J., Browne, A., and Johnson, N. "Effect of bending on the performance of spool-packaged shape memory alloy actuators", Proc. SPIE (2009).

[8] Sun, H., Pathak, A., Luntz, J., Brei, D., Alexander, P., Johnson, N. “Stabilizing shape memory alloy actuator performance through cyclic shakedown: An empirical study”, Proc. SPIE (2008)